Journal of Medicinal Chemistry

Article

Drug Discovery against Psoriasis: Identification of a New Potent FMS-like Tyrosine Kinase 3 (FLT3) Inhibitor, 1-(4-((1H-pyrazolo[3,4-d]pyrimidin-4-yl)oxy)-3-fluorophenyl)-3-(5-(tert-butyl)isoxazol-3-yl)urea, That Showed Potent Activity in a Psoriatic Animal Model

Guo-Bo Li, Shuang Ma, Ling-Ling Yang, Sen Ji, Zhen Fang, Guo Zhang, Li-Jiao Wang, Jie-Min Zhong, Yu Xiong, Jiang-Hong Wang, Shen-Zhen Huang, Lin-Li Li, Rong Xiang, Dawen Niu, Ying-Chun Chen, and Sheng-Yong Yang

J. Med. Chem., **Just Accepted Manuscript** • DOI: 10.1021/acs.jmedchem.6b00604 • Publication Date (Web): 18 Aug 2016

Just Accepted

ACS Publications

Journal of Medicinal Chemistry is published by the American Chemical Society. 1155 Sixteenth Street N.W., Washington, DC 20036

	University Niu, Dawen; State Key Laboratory of Biotherapy and Cancer Center, West China Hospital, Sichuan University/Collaborative Innovation Center of Biotherapy Chen, Ying-Chun; Key Laboratory of Drug Targeting and Drug Delivery System of Ministry of Education, West China School of Pharmacy, Sichuan University Yang, Sheng-Yong; State Key Laboratory of Biotherapy and Cancer Center, West China Hospital, Sichuan University/Collaborative Innovation Center of Biotherapy

Drug Discovery against Psoriasis: Identification of a New Potent FMS-like Tyrosine Kinase 3 (FLT3) Inhibitor, 1-(4-((1*H*-pyrazolo[3,4-*d*]pyrimidin-4-yl)oxy) -3-fluorophenyl)-3-(5-(tert-butyl)isoxazol-3-yl)urea, That Showed Potent Activity in a Psoriatic Animal Model

Guo-Bo Li,[†,#] Shuang Ma,[†,#] Ling-Ling Yang,[†,‡] Sen Ji,[†] Zhen Fang,[†] Guo Zhang,[§] Li-Jiao Wang,[†,‡] Jie-Min Zhong,[†] Yu Xiong,[†] Jiang-Hong Wang,[§] Shen-Zhen Huang,[†] Lin-Li Li,[§] Rong Xiang,[&] Dawen Niu,[†] Ying-Chun Chen,[§] and Sheng-Yong Yang[†,*]

[†] *State Key Laboratory of Biotherapy and Cancer Center, West China Hospital, Sichuan University/Collaborative Innovation Center of Biotherapy, Sichuan 610041, China*

[‡] *College of Food and Bioengineering, Xihua University, Sichuan 610039, China*

[§] *Key Laboratory of Drug Targeting and Drug Delivery System of Ministry of Education, West China School of Pharmacy, Sichuan University, Chengdu, Sichuan, 610041, China*

[&] *Department of Clinical Medicine, School of Medicine, Nankai University, Tianjin, China*

Abstract

Psoriasis is a chronic T-cell-mediated autoimmune disease, and FMS-like tyrosine kinase 3 (FLT3) has been considered as a potential molecular target for the treatment

of psoriasis. In this investigation, structural optimization was performed on a lead compound, 1-(4-(1*H*-pyrazolo[3,4-*d*]pyrimidin-4-yloxy)phenyl)-3-(4-chloro-3-(trifluoromethyl)phenyl)urea (**1**), which showed a moderate inhibitory activity againt FLT3. A series of pyrazolo[3,4-*d*]pyrimidine derivatives were synthesized, and structure-activity relationship analysis led to the discovery of a number of potent FLT3 inhibitors. One of the most active compounds, 1-(4-(1*H*-pyrazolo[3,4-*d*]pyrimidin-4-yloxy)-3-fluorophenyl)-3-(5-tert-butylisoxazol-3-yl)urea (**18b**), was then chosen for in-depth anti-psoriasis studies because this compound displayed the highest potency in a preliminary anti-psoriasis test. Compound **18b** exhibited significant anti-psoriatic effects in the K14-VEGF transgenic mouse model of psoriasis, and no recurrence was found 15 days later after the last administration. Detailed mechanisms of action of compound **18b** were also investigated. Collectively, compound **18b** could be a potential drug candidate for psoriasis treatment.

1. Introduction

Psoriasis is a long-lasting autoimmune disease characterized by itchy, scaly, and erythematous skin patches, which has profound psychological effects on patients and their family members.[1,2] Though the pathogenesis of psoriasis has not been fully understood, significant evidence indicates that psoriasis is highly related to the inappropriate or unregulated activation of autoreactive T cells.[1,3] Traditional approaches for psoriasis treatment through immunosuppression have thus focused on the direct inhibition of T cells. However, these treatments inevitably cause considerable toxic side effects, including immunogenicity and immunosuppression of beneficial immune responses.[3-5] Therefore, safe and effective strategies for the treatment of psoriasis are in great demand at present.

Recent studies have shown that targeted inhibition of antigen-presenting cells could be a safe and effective approach to treat autoimmune diseases including psoriasis.[4,6-10] Dendritic cells (DCs) are the main antigen-presenting cells for regulating immune responses.[11-14] On the one hand, DCs can effectively activate T cells to mediate immune response by ingesting, processing and presenting the antigens to T cells.[15,16] On the other hand, DC-T-cell interactions drive the differentiation of T cells towards specific phenotypes. For instance, DCs can stimulate the T cells to differentiate into Th17 cells, which are thought to play an essential role in the pathogenesis of autoimmune diseases, through secreting cytokines, including interleukin-23 (IL-23), transforming growth factor β (TGF-β), and interleukin-6 (IL-6).[17,18] Thus, targeted inhibition of DCs may provide a new and effective therapeutic strategy for psoriasis treatment by down-regulating the T-cell-mediated immune responses. Furthermore, it has been demonstrated that the FMS-like tyrosine kinase 3 (FLT3) plays a critical role in regulating the generation and maturation of

DCs.[19] FLT3 is known to express in hematopoietic progenitors,[20,21] and stimulation of FLT3 via its ligand either *in vitro* or *in vivo* could drive the expansion and differentiation of hematopoietic progenitors towards to a DC phenotype.[22-24] FLT3 is also highly expressed in mature DCs,[25] suggesting that signals through this receptor could be an important aspect of maintaining DC function. In a recent study, Whartenby *et al* reported that inhibition of FLT3 signaling could induce apoptosis in both mouse and human DCs.[26] Additionally, we for the first time detected a significant accumulation of $FLT3^+$ DCs in human psoriatic lesions compared with normal skin from same psoriasis patients.[27] All of these studies indicate that FLT3 is likely a potential molecular target for the treatment of psoriasis through interference with DCs.

We previously disclosed an FLT3 inhibitor, 1-(4-(1*H*-pyrazolo[3,4-*d*]pyrimidin-4-yloxy)phenyl)-3-(4-chloro-3-(trifluoromethyl)phenyl)urea (**1**, Figure 1a),[28] which showed an IC_{50} value of 39 nM against FLT3. This compound indeed exhibited certain anti-psoriatic effect in vascular endothelial growth factor (K14-VEGF) transgenic homozygous mice; the K14-VEGF transgenic mouse model is one of the most commonly used psoriasis models, which can develop a cutaneous inflammatory condition resembling psoriasis.[29-32] Nevertheless, the activity was at a moderate level, which could be mainly due to the moderate potency against FLT3 of this compound. We shall in this investigation perform a further structural modification to improve its potency against FLT3. The structure-activity relationship (SAR) will also be discussed. The most active compounds will be evaluated for their anti-psoriatic effects *in vivo*, and mechanisms of action will be examined as well.

<Figure 1 here>

2. Results and Discussion

2.1 Synthesis of 4-Phenoxy-1*H*-pyrazolo[3,4-*d*]pyrimidine Derivatives

All target compounds were prepared by routes outlined in Schemes 1-5. Scheme 1 shows the synthetic routes for compounds **7a-c**. Firstly, the regioisomeric 3- and 5-aminoisoxazole intermediates **4a-c** were synthesized in slightly different ways. The 3-aminoisoxazoles **4a** and **4c** were obtained by initial attack of the hydroxylamine nitrogen on the cyano group of the ketonitriles (**3a** and **3b**) at pH 7-8 at 55 ℃, followed by ring closure under acidic conditions (pH 3-4) at 55 ℃. The 5-aminoisoxazole **4b** was acquired by initial attack of the hydroxylamine nitrogen on the ketone group of 4,4-dimethyl-3-oxopentanenitrile (**3a**) and ring closure at pH 8 at 100 ℃ for 2.5 h. Secondly, reaction of 4-chloro-1*H*-pyrazolo[3,4-*d*]pyrimidine (**5**) with 4-aminophenolate through nucleophilic substitution produced intermediate 4-(1*H*-pyrazolo[3,4-*d*]pyrimidin-4-yloxy)aniline (**6**). Finally, treatment of 3- or 5-aminoisoxazoles **4a-c** with triphosgene led to corresponding isocyanates using a similar method as that described in our previous work.[33] The resulting isocyanates then reacted with **6** to give final products **7a-c** in 58-89% yields.

<Scheme 1 here>

The general synthetic routes for compounds **9a-f**, which contain a substituted pyrazole group in ring B, are depicted in Scheme 2. Esters **2a-c** reacted with acetonitrile to produce ketonitriles **3a-c** in 68%-84% yields. Intermediates **8a-f** were then obtained through a ring closure process of **3a-c** with alkyl or aryl hydrazines. The hydrazines used here were commercially available or synthesized, and cyclopentylhydrazine was synthesized according to the method described by

Ranatunge *et al.*[34] The target compounds **9a-f** were finally synthesized from **8a-f** using a method similar to that for **7a-c** in 58%-92% yields.

<Scheme 2 here>

Scheme 3 presents the synthetic routes for compounds **12a**, **12b** and **14**. Commercially available 1-chloro-3,3-dimethylbutan-2-one (**10a**) and 2-bromo-1-phenylethanone (**10b**) reacted with thiocarbamide in EtOH at 90 ℃ to produce 2-aminothiazoles **11a** and **11b**, respectively. Treatment of **11a**, **11b** and benzo[*d*]thiazol-2-amine (**13)**, which was purchased from the market, with triphosgene in the presence of triethylamine afforded the corresponding isocyanates, which then reacted with 4-(1*H*-pyrazolo[3,4-*d*]pyrimidin-4-yloxy)aniline (**6**) to produce the desired products **12a**, **12b** and **14** in good yields.

<Scheme 3 here>

Synthetic routes for compounds **16a-d** are displayed in Scheme 4. Compounds **16a** and **16b**, which contain a methyl or isopropyl substituent at the *N*-1 of pyrazolopyrimidine, were prepared from the corresponding analogue **7a** in the presence of sodium hydroxide in *N*,*N*-dimethylformamide (DMF) at room temperature and 60 ℃, respectively. Compounds **16c** and **16d** were obtained using a two-step procedure involving substitution of the 1-*NH* of 4-(1*H*-pyrazolo[3,4-*d*]pyrimidin-4-yloxy)aniline (**6**) by 3-chloro-*N*,*N*-dimethylpropan-1-amine or 4-(2-chloroethyl)morpholine in DMF at 100 ℃ under basic conditions and subsequent formation of ureas as described above.

<Scheme 4 here>

Scheme 5 shows the synthetic routes for compounds **18a-e**, **19a-d**, and **20**. Reactions of 4-chloro-1*H*-pyrazolo[3,4-*d*]pyrimidine (**5**) with various 2- or 3-substituted 4-aminophenols gave intermediates **17a-e** in the presence of sodium hydroxide. Compounds **18a-e** were then prepared by reaction of intermediates **17a-e** with 5-(tert-butyl)isoxazol-3-amine (**4a**), respectively, with yields ranging from 51% to quantitative. Compounds **19a-d** and **20** bearing a pyrazole-urea moiety were synthesized using corresponding pyrazoleisocyanates and intermediate **17b** at a temperature of 120 ℃.

<Scheme 5 here>

2.2 SAR of 4-Phenoxy-1*H*-pyrazolo[3,4-*d*]pyrimidine Derivatives

2.2.1 Variation of the 3-Position of the Urea Moiety (Ring B)

In our previous study, we found that the substituent of 3-position of the urea moiety (ring B, Figure 1b) of compound **1** has a significant influence on the activity against FLT3. Therefore, in this investigation, various substituted 5-membered aromatic heterocyclic rings were used to replace the original ring B. The inhibitory potencies (IC_{50}) against FLT3 of the synthesized compounds **7a-c**, **9a-f**, **12a-b**, and **14** are shown in Table 1. From Table 1, we can see that compounds **7a**, **7b**, **9c**, and **12a**, containing regioisomeric 5-(tert-butyl)isoxazole, 3-(tert-butyl)isoxazole, 3-(tert-butyl)-1*H*-pyrazole-1-carboxylic acid, and 4-(tert-butyl)-thiazole, respectively, displayed 3- or 4-fold more potent activity against FLT3 (IC_{50}: 11nM, 8nM, 10nM, and 8nM, respectively) than compound **1**. In contrast, compounds **9b**, **9d**, **12b**, and **14**, containing a heterocyclic ring with larger substituents at ring B, showed decreased

activities. Especially, compound **14** with a phenyl-substituted thiazole ring exhibited significantly reduced ability to inhibit FLT3. We noticed that the most potent derivatives **7a**, **7b**, and **12a** actually have highly similar substituents at ring B, which are 5-(tert-butyl)isoxazole, 3-(tert-butyl)isoxazole, and 4-(tert-butyl)-thiazole, respectively. Considering that 5-(tert-butyl)isoxazole has often been used as a key motif in drugs or drug candidates like Quizartinib, implying a good biocompatibility, we thus chose the 5-(tert-butyl)isoxazole moiety as an optimal substituent for further structural optimization.

<**Table 1 here**>

2.2.2 Substitution of the *N*-1 Position of Pyrazolo[3,4-*d*]pyrimidine

To examine the substitution effect of the *N*-1 position in the pyrazolo[3,4-*d*]pyrimidine moiety, we introduced various substituents at this position and fixed the 3-position of the urea moiety as the optimal 5-(tert-butyl)isoxazole group. Inhibitory activities of the synthesized compounds **16a-d** are presented in Table 2. Obviously, either large (**16c**, **16d**) or small (**16a**, **16b**) substitution at the *N*-1 position negatively affected the inhibitory activities against FLT3. Therefore, the *NH* in the pyrazolo[3,4-*d*]pyrimidine moiety may be an important pharmacophore for binding with FLT3, and substitution at the *N*-1 position of pyrazolo[3,4-d]pyrimidine is not beneficial for the inhibitory activity improvement.

<**Table 2 here**>

2.2.3 Replacement on the 1-Phenyl Group of the Urea Moiety (Ring A)

We further examined the possible influences of substitutions on the 1-phenyl

group of the urea moiety (Figure 1b, ring A). The ring B moiety was still fixed as the optimal 5-tert-butyl-isoxazole group, and no substitution occurred at the *N*-1 position of pyrazolo[3,4-*d*]pyrimidine. The inhibitory activities of synthesized target compounds **18a-e**, in which different substituents were attached to the 2- or 3-position of ring A, are shown in Table 3. Compounds **18b**, **18c**, and **18e** with the 2-position of ring A replaced by fluoride, chlorine or methyl exhibited more potent activities against FLT3 than unsubstituted **7a**. Compared with substitution at the 2-position of ring A, substitution at the 3-position of ring A is less favorable for the inhibitory activity, particularly substitution by a bulky group (for example, see **18d** vs **18e**). From here, a preliminary conclusion might be made that substitution at the 2-position of ring A by fluoride or chlorine helps to enhance the bioactivity of target compounds. To examine this point, we synthesized several other compounds, in which the 2-position of ring A was substituted with fluoride and ring B was replaced by other 5-membered aromatic heterocyclic rings, including 3-tert-butyl-1-methyl-1*H*-pyrazole (**19a**), 3-tert-butyl-1-phenyl-1*H*-pyrazole (**19b**), 3-tert-butyl-1-cyclopentyl-1*H*-pyraz-ole (**19c**), 3-tert-butyl-1-(4-fluorophenyl)-1*H*-pyrazole (**19d**), and 1-methyl-3-(trifluoromethyl)-1*H*-pyrazole (**20**). Bioactivities of these compounds are also shown in Table 3. From Table 3, we can see that compounds containing substituent fluorine at the 2-position of ring A only exhibited comparable potencies compared with their counterparts (**19a** vs **9a**, **19b** vs **9d**, **19c** vs **9b**, and **20** vs **9e**). These results imply that substitution at the 2-position of ring A by fluoride or chlorine

does not mean that it must help to significantly improve the bioactivity of target compounds.

<**Table 3 here**>

Collectively, the structural optimization and SAR studies led to the discovery of a number of novel compounds that exhibited a higher potency against FLT3 than original lead compound **1**. We then chose five most active compounds, namely **7b**, **12a**, **18a**, **18b**, and **18c**, to perform a preliminary *in vivo* anti-psoriasis study with the K14-VEGF transgenic mouse model. All of these compounds showed good anti-psoriatic activity in this model, and compound **18b** is the most potent one. Therefore, further in-depth studies of anti-psoriasis and mechanisms of action were subsequently carried out on compound **18b**.

2.3 *In Vitro* Effects of Compound 18b on Plasmacytoid DCs and Myeloid DCs

The plasmacytoid DCs (pDCs) and myeloid DCs (mDCs) are two main subpopulations of immature DCs, both of which are highly aggregated in psoriatic lesions.[27] We first examined the effects of compound **18b** on the generation of pDCs and mDCs *in vitro*. For this purpose, mature bone marrow-derived cells (BMDCs) were separated and cultured according to a standard protocol as described in materials and methods section. The FLT3 ligand (FLT3L) was supplemented to BM culture to induce the generation of $FLT3^+$ $CD11c^+$ DCs as described previously.[35] As shown in Figure 2a, the numbers of pDCs and mDCs were reduced after compound **18b** treatment. These results indicate that compound **18b** could suppress the generation of pDCs and mDCs from BMDCs.

<Figure 2 here>

Because DCs (pDCs and mDCs) may have impact on the differentiation of T cells towards Th1 and Th17 cells through secretion of certain cytokines,[4,36-38] we next assessed the influence of compound **18b** on secretion of cytokine interferon (IFN)-γ and IL-23 in the culture system of DCs. Using the same protocol described above, DCs were induced with FLT3L with or without addition of compound **18b** and the supernatants were detected by Elisa. As shown in Figure 2b, compound **18b** could dramatically decrease IFN-γ and IL-23 levels even at 10 nM.

We then further examined the effects of compound **18b** on the key downstream signaling components of FLT3 pathway including signal transducer and activator of transcription 3 and 5 (STAT3 and STAT5), which are critical transcription factors involved in production of many inflammatory cytokines.[39,40] The results from western blot analysis showed that the phosphorylation and activation of STAT3 and STAT5 in DCs were decreased after compound **18b** treatment for 1 h (Figure 2c). Taken together, these results indicated that compound **18b** could decrease the number of DCs and inhibit cytokine secretion of DCs through the blockade of FLT3 signaling pathway.

2.4 *In Vivo* Effects of Compound 18b on K14-VEGF Transgenic Mice

The *in vivo* anti-psoriatic effects of compound **18b** were evaluated using the transgenic K14-VEGF mice. The heavy symptom K14-VEGF mice were treated with compound **18b** or vehicle by smearing over the lesion surface uniformly. As shown in Figure 3a, after a continuous treatment of **18b** for 21 days, an obvious improvement of psoriatic symptom was observed in the compound **18b** treated group compared

with the vehicle group. There was no recurrence 15 days later after the last administration. Histology also showed that compound **18b** treatment led to a significant alleviation in the psoriatic disease indexes including epidermal thickness, focal parakeratosis, lack of granular layer, and abundant infiltrated lymphocytes (Figure 3b). This was further confirmed by the Baker scores (Figure 3c); the Baker score system is a traditional evaluation method in skin disease. From Figure 3c, we can see that the pathological scores of the mice treated with compound **18b** were significantly decreased compared with those of the vehicle-treated controls. Thus we conclude that compound **18b** could effectively alleviated psoriasis in K14-VEGF transgenic mice.

<**Figure 3 here**>

2.5 Mechanisms of Action of Compound 18b

The mechanisms of action underlying the *in vivo* anti-psoriatic effects of compound **18b** were further examined. Firstly, we examined the direct effect of compound **18b** on the population of $FLT3^+$ $CD11c^+$ DCs (pDCs and mDCs) in K14-VEGF transgenic mice, because it has been shown that a high expression of FLT3 and a significant accumulation of $FLT3^+$ $CD11c^+$ DCs are typical characteristics of psoriatic lesions.[27,41] After external administration of compound **18b** to the K14-VEGF mice for 29 days, we tested the number of $FLT3^+$ $CD11c^+$ DCs in psoriatic lesions by flow cytometric quantifications. As shown in Figure 4a, the number of $FLT3^+$ $CD11c^+$ DCs in the skin was significantly decreased (about 69.6%) in compound **18b**-treated mice compared with control group mice. The populations of

pDCs and mDCs in $FLT3^+$ $CD11c^+$ DCs were further analyzed. We found that the numbers of $FLT3^+$ $CD11c^+$ $B220^+$ DCs (pDCs) and $FLT3^+$ $CD11c^+$ MHC class II^+ DCs (mDCs) were both greatly reduced in compound **18b**-treated mice compared with those in vehicle-treated mice (Figure 4b).

<**Figure 4 here**>

Secondly, we examined the effects of compound **18b** on the defining histological features of psoriasis including marked infiltration of T cells, elongated/hyperplastic blood vessels, and the presence of various pro-inflammatory cytokines, chemokines, and growth factors in the vehicle-treated and compound **18b**-treated psoriatic lesions. As shown in Figure 5, compound **18b** treatment significantly reduced the expressions of CD8, CD31, VEGF, CD54, and phosphorylated STAT3 (pSTAT3) compared with vehicle treatment. The decrease in CD8 (79%) indicates inhibition of the infiltration of $CD8^+$ inflammatory lymphocytes. The percent of CD31 and VEGF expression were reduced about 94% and 90% respectively, implying that compound **18b** suppressed the proliferation and dilation of blood vessels. The reduction of expression of CD54 was about 87%, which indicates a decrease in endothelial cell activation. Finally, the reduction in pSTAT3 (64%) expression implies the inhibition of keratinocyte hyper proliferation. Taken together, these results showed that compound **18b** could suppress the infiltration of T cells, the abnormal growth of blood vessels, and the expression of pro-inflammatory chemokines and growth factors in psoriatic lesions.

<**Figure 5 here**>

Finally, we examined the impact of compound **18b** on cytokines related to Th17/Th1 pathways, because psoriasis is thought to be a mixed Th17/Th1 disease.[42-44] Flow cytometric analysis showed that the number of Th17 (IL-17$^+$ CD4$^+$) cells in the lymph nodes was considerably lower in the compound **18b**-treated group compared with the vehicle-treated group (Figure 6a). The expressions of IFN-γ and IL-17 in blood were also significantly down-regulated by compound **18b**, as IFN-γ and IL-17 are thought to be produced by Th1 and Th17 inflammatory pathway, respectively. These results indicated that compound **18b** treatment suppressed the Th17/Th1 pathways.

<**Figure 6 here**>

3. Concluding Remarks

In this investigation, a series of 4-phenoxy-1*H*-pyrazolo[3,4-*d*]pyrimidine derivatives were synthesized. SAR studies led to discovery of a number of potent FLT3 inhibitors. One of the most potent FLT3 inhibitors, compound **18b**, showed the highest anti-psoriatic activity in a preliminary *in vivo* anti-psoriasis study. This compound was then carried out further in-depth *in vitro* and *in vivo* anti-psoriatic studies. The *in vitro* results indicated that compound **18b** could reduce the generation of DCs and inhibit cytokine secretion of DCs through the blockade of FLT3 signaling pathway. The *in vivo* studies showed that compound **18b** could effectively alleviate psoriasis in K14-VEGF transgenic mice. The mechanism of action studies revealed that compound **18b** could suppress the population of FLT3$^+$ CD11c$^+$ DCs (including pDCs and mDCs), the infiltration of T-cell, and the levels of related pro-inflammation

chemokines and growth factors, as well as the expression of cytokines related to Th17/Th1 pathways. Collectively, compound **18b** obtained here could be a potential drug candidate for the treatment of psoriasis.

4. Experimental Section

Chemistry Methods

Unless otherwise noted, all starting materials, reagents, and solvents were purchased from commercial vendors and used as supplied without further purification. Reactions were monitored by thin layer chromatography (TLC) on Merck silica gel 60 F-254 thin layer plates. ^{1}H NMR and ^{13}C NMR spectra were recorded on a Bruker AV-400 spectrometer at 400 MHz and 100 MHz, respectively. Chemical shifts (δ) are expressed in parts per million (ppm) relative to tetramethylsilane (TMS) as an internal standard. The following abbreviations are used to designate multiplicities: s, singlet; d, doublet; t, triplet; q, quartet; m, multiplet; dd, double–doublet; br s, broad signal. Low-resolution and high-resolution mass spectral (MS) data were determined on an Agilent 1100 Series LC-MS with UV detection at 254 nm in low-resonance electrospray ionization (ESI) mode. All the final compounds were purified to >95% purity, as determined by high-performance liquid chromatography (HPLC). HPLC analysis was performed on a Waters 2695 HPLC system equipped with a Kromasil C18 column (4.6 mm × 250 mm, 5 um).

1-(4-(1*H*-pyrazolo[3,4-*d*]pyrimidin-4-yloxy)phenyl)-3-(5-tert-butylisoxazol-3-yl)urea (7a) The chemical sythesis of intermediate **6** builds upon previously

published method.[28] ^{1}H NMR (400 MHz, DMSO-d_6): δ 14.07 (s, 1H), 8.50 (s, 1H), 7.67 (s, 1H), 6.96 (d, *J*=8.8 Hz, 2H), 6.64 (d, *J*=8.8 Hz, 2H), 5.20 (s, 2H) ppm; LC-MS m/z: 228.1 $[M + H]^+$.

A solution of 5-(tert-butyl)isoxazol-3-amine (**4a**, 0.308 g, 2.2 mmol) dissolved in THF (20 ml) was slowly dripped into a stirred solution of triphosgene (0.654 g, 2.2 mmol) in THF (5 mL) using a constant pressure dropping funnel at room temperature. Triethylamine (0.65 mL, 4.6 mmol) was then added slowly to the reaction mixture after the aniline was completely added. Subsequently, the reaction was reflux for 2 hours. After evaporation of the solvent, the residue was dissolved in acetonitrile (20 ml) and toluene (20 ml), and compound **6** (0.454 g, 2.0 mmol) was added. Next, the reaction mixture was stirred at 110 ℃ for 16 h, and the solvent was removed *in vacuo*. The residue obtained was purified by column chromatography (eluent gradient CH_2Cl_2:MeOH, 60:1) and recrystallized from EtOAc and petroleum ether. Yield: 89%, 95.9% HPLC purity. ^{1}H NMR(400 MHz, DMSO-d_6): δ 14.13 (s, 1H), 9.55 (s, 1H), 8.95 (s, 1H), 8.51 (s, 1H), 8.05 (s, 1H), 7.56 (d, *J*=8.8 Hz, 2H), 7.27 (d, *J*=8.8 Hz, 2H), 6.52 (s, 1H), 1.30 (s, 9H) ppm; ^{13}C NMR (100 MHz, DMSO-d_6): δ 180.7, 163.6, 158.9, 157.2, 155.4, 151.9, 147.4, 137.3, 132.3, 122.8, 120.2, 101.8, 93.0, 33.0, 28.8 ppm; HRMS (m/z): calcd for $C_{19}H_{20}N_7O_3$ $[M + H]^+$ 394.1622, found 394.1604; $C_{19}H_{19}N_7NaO_3$ $[M + Na]^+$ 416.1442, found 416.1419.

1-(4-(1*H*-pyrazolo[3,4-*d*]pyrimidin-4-yloxy)phenyl)-3-(3-tert-butylisoxazol-5-yl)urea (7b) The title compound was synthesized in a manner similar to the synthesis of **7a** using compounds **4b** and **6** to give compound **7b**, which was purified by column

chromatography (eluent gradient CH_2Cl_2:MeOH, 60:1) and recrystallized from EtOAc and petroleum ether. Yield: 80%, 95.9% HPLC purity. ^{1}H NMR (400 MHz, DMSO-d_6): δ 14.14 (s, 1H), 9.56 (s, 1H), 8.94 (s, 1H), 8.51 (s, 1H), 8.06 (s, 1H), 7.56 (d, *J*=8.8 Hz, 2H), 7.27 (d, *J*=8.8 Hz, 2H), 6.52 (s, 1H), 1.30 (s, 9H) ppm; ^{13}C NMR (100 MHz, DMSO-d_6): δ 180.2, 163.1, 158.3, 156.7, 154.9, 151.4, 146.9, 136.8, 131.8, 122.3, 119.7, 101.3, 92.4, 32.4, 28.3 ppm; HRMS (m/z): calcd for $C_{19}H_{20}N_7O_3$ $[M + H]^+$ 394.1622, found 394.1604; $C_{19}H_{19}N_7NaO_3$ $[M + Na]^+$ 416.1442, found 416.1419.

1-(4-(1*H*-pyrazolo[3,4-*d*]pyrimidin-4-yloxy)phenyl)-3-(3-tert-butyl-1-cyclopentyl-1*H*-pyrazol-5-yl)urea (9b) A mixture of cyclopentanone (0.84 g, 10 mmol) and tert-butyl hydrazinecarboxylate (1.32 g, 10 mmol) in methanol (50 ml) was stirred at ambient temperature for 3 h. Subsequently, the solvent was removed *in vacuo*, and tert-butyl 2-cyclopentylidenehydrazinecarboxylate (1.92 g) was obtained as a white solid in high yield.

Tert-butyl-2-cyclopentylidene-hydrazinecarboxylate (1.92 g, 9.7 mmol) was dissolved in 50% acetic acid (30 ml). The resulting solution was then stirred at room temperature for 2.5 h after the portion wise addition of sodium cyanoborohydride (0.60 g, 9.6 mmol). The reaction mixture was neutralized with NaOH and extracted with CH_2Cl_2, and the organic layer was dried with anhydrous $MgSO_4$ and evaporated to give the reduction product as oil (1.7 g). The product was used without further purification.

Trifluoroacetic acid (10 ml) was added dropwise to a solution of tert-butyl

2-cyclopentyl-hydrazinecarboxylate (1.7 g, 8.55 mmol) in CH_2Cl_2 (10 ml). The solution was stirred at ambient temperature for 1.5 h. The solvent was then evaporated to give the trifuoroacetate salt as colorless oil in high yield.

3-Tert-butyl-1-cyclopentyl-1*H*-pyrazol-5-amine **(8b)** was synthesized from 4,4-dimethyl-3-oxopentanenitrile (**3a**) and the trifuoroacetate salt of cyclopentylhydrazine using a procedure similar to that of **8a** (Yield:76%).

The title compound was prepared from **8b** and **6** using the procedure described above for compound **7a**, which was purified by column chromatography (eluent gradient CH_2Cl_2:MeOH, 55:1) and purified by recrystallization from EtOAc and petroleum ether. Yield: 92%, 97.4% HPLC purity. ^{1}H NMR(400 MHz, DMSO-d_6): δ 14.15 (s, 1H), 9.38 (s, 1H), 8.79 (s, 1H), 8.51 (s, 1H), 8.03 (s, 1H), 7.56 (d, *J*=8.0 Hz, 2H), 7.24 (d, *J*=8.0 Hz, 2H), 6.05 (s, 1H), 4.63-4.55 (m, 1H), 1.99-1.92 (m, 4H), 1.84-1.81 (m, 2H), 1.60-1.56 (m, 2H), 1.22 (s, 9H) ppm; ^{13}C NMR (100 MHz, DMSO-d_6): δ 162.8, 159.3, 157.0, 155.3, 149.6, 138.5, 133.8, 132.0, 124.8, 116.9, 107.2, 101.6, 96.6, 57.5, 32.4, 30.9, 24.4 ppm; HRMS (m/z): calcd for $C_{24}H_{29}N_8O_2$ [M + H]$^+$ 461.2408, found 461.2410; $C_{24}H_{28}N_8NaO_2$ [M + Na]$^+$ 483.2227, found 483.2232.

1-(4-(1*H*-pyrazolo[3,4-*d*]pyrimidin-4-yloxy)phenyl)-3-(4-tert-butylthiazol-2-yl)urea (12a) A mixture of 1-chloro-3,3-dimethylbutan-2-one (**10a**, 2.0 ml, 15.2 mmol) andthiocarbamide (1.16 g, 15.2 mmol) was reacted for 12 h in refluxed alcohol. Solvent was evaporated to give the crude product 4-(tert-butyl)thiazol-2-amine (**11a**); Yield: 88%.

The title compound was synthesized in a manner similar to the synthesis of **7a** using compounds **11a** and **6** to give compound **12a**, which was purified by column chromatography (eluent gradient CH_2Cl_2:MeOH, 60:1) and recrystallized from EtOAc and petroleum ether. Yield: 76%, 100% HPLC purity. ^{1}H NMR (400 MHz, DMSO-d_6): δ 14.13 (s, 1H), 10.65 (s, 1H), 8.96 (s, 1H), 8.51 (s, 1H), 8.06 (s, 1H), 7.57 (d, *J*=8.8 Hz, 2H), 7.28 (d, *J*=8.8 Hz, 2H), 6.65 (s, 1H), 1.26 (s, 9H) ppm; ^{13}C NMR (100 MHz, DMSO-d_6): δ 180.7, 164.0, 158.9, 157.3, 155.4, 151.9, 147.4, 137.3, 132.3, 122.8, 120.2, 103.4, 93.0, 33.0, 28.8 ppm; HRMS (m/z): calcd for $C_{19}H_{20}N_7O_2S$ $[M + H]^+$ 410.1394, found 410.1383; $C_{19}H_{19}N_7NaO_2S$ $[M + Na]^+$ 432.1213, found 432.1208.

1-(5-Tert-butylisoxazol-3-yl)-3-(4-(1-(2-morpholinoethyl)-1*H*-pyrazolo[3,4-*d*] pyrimidin-4-yloxy)phenyl)urea (16d) The title compound was synthesized in a manner similar to the synthesis of **16c** using compounds **15b** and **4a** to give compound **16d**, which was purified by column chromatography (eluent gradient CH_2Cl_2:MeOH, 40:1) and recrystallized from EtOAc and petroleum ether. Yield: 76%, 97.9% HPLC purity. ^{1}H NMR (400 MHz, DMSO-d_6): δ 9.57 (s, 1H), 9.04 (s, 1H), 8.54 (s, 1H), 8.10 (s, 1H), 7.56 (d, *J*=8.8 Hz, 2H), 7.27 (d, *J*=8.8 Hz, 2H), 6.51 (s, 1H), 4.56 (br s, 2H), 3.46 (s, 4H), 2.80 (s, 2H), 2.43 (s, 4H), 1.30 (s, 9H) ppm; ^{13}C NMR (100 MHz, DMSO-d_6): δ 180.7, 163.7, 158.8, 155.6, 155.3, 151.9, 147.3, 137.4, 131.8, 122.8, 120.2, 100.2, 93.0, 66.6, 57.5, 53.4, 33.9, 28.8 ppm; HRMS (m/z): calcd for $C_{25}H_{31}N_8O_4$ $[M + H]^+$ 507.2463, found 507.2462; $C_{25}H_{30}N_8NaO_4$ $[M + Na]^+$ 529.2282, found 529.2277.

1-(4-(1*H*-pyrazolo[3,4-*d*]pyrimidin-4-yloxy)-2-fluorophenyl)-3-(5-tert-butylisoxazol-3-yl)urea (18a) Sodium hydroxide (0.20 g, 5.0 mmol) was added to a solution of 4-amino-3-fluorophenol (0.635 g, 5.0 mmol) in H_2O (20 ml). The mixture was stirred at room temperature for 30 minutes. Then, 4-chloro-1*H*-pyrazolo[3,4-*d*]pyrimidine (**5**, 0.77 g, 5.0 mmol) in THF (20 ml) was slowly added, and the reaction mixture was heated to 60 ℃ for 2 hours. The solvent was then partially evaporated on a rotary evaporator. The obtained crude mixture was extracted with ethyl acetate (2 × 120 ml) and water. The combined organic layers were dried over $MgSO_4$ and concentrated, and the residue was purified by column chromatography (eluent gradient CH_2Cl_2:MeOH, 80:1) without final recrystallization to give **17a** (0.502 g, 41%) as a brown solid.

The title compound was synthesized in a manner similar to the synthesis of **7a** using compounds **17a** and **4a** to give compound **18a**, which was purified by column chromatography (eluent gradient petroleum ether:EtOAc, 3:1) and recrystallized from EtOAc and petroleum ether. Yield: 51%, 97.4% HPLC purity. ^{1}H NMR (400 MHz, DMSO-d_6): δ 14.17 (s, 1H), 9.86 (s, 1H), 8.87 (s, 1H), 8.52 (s, 1H), 8.19-8.15 (m, 2H), 7.44 (d, *J*=10.4 Hz, 1H), 7.16 (d, *J*=8.4 Hz, 1H), 6.50 (s, 1H), 1.29 (s, 9H) ppm; ^{13}C NMR (100 MHz, DMSO-d_6): δ 180.8, 163.2, 158.7, 157.2, 155.3, 153.8, 151.7, 147.2, 132.2, 121.9, 118.6, 110.5, 101.8, 92.8, 32.9, 28.8 ppm; HRMS (m/z): calcd for $C_{19}H_{18}FN_7NaO_3$ $[M + Na]^+$ 434.1347, found 434.1351.

1-(4-(1*H*-pyrazolo[3,4-*d*]pyrimidin-4-yloxy)-3-fluorophenyl)-3-(5-tert-butylisoxazol-3-yl)urea (18b) The title compound was synthesized in a manner similar to

the synthesis of **7a** using compounds **17b** and **4a** to give compound **18b**, which was purified by column chromatography (eluent gradient petroleum ether:EtOAc, 3:1) and recrystallized from EtOAc and petroleum ether. Yield: 89%, 98.6% HPLC purity. ^{1}H NMR (400 MHz, DMSO-d_6): δ 14.24 (s, 1H), 9.65 (s, 1H), 9.14 (s, 1H), 8.53 (s, 1H), 8.31 (s, 1H), 7.70 (d, *J*=10.8 Hz, 1H), 7.42 (t, *J*=8.4 Hz, 1H), 7.24 (d, *J*=9.2 Hz, 1H), 6.53 (s, 1H), 1.31 (s, 9H) ppm; ^{13}C NMR (100 MHz, DMSO-d_6): δ 180.8, 162.6, 158.7, 157.2, 155.3, 152.8, 151.9, 138.2, 133.9, 132.2, 124.8, 115.3, 107.4, 101.4, 93.1, 33.0, 28.8 ppm; HRMS (m/z): calcd for $C_{19}H_{19}FN_7O_3$ $[M + H]^+$ 412.1528, found 412.1511; $C_{19}H_{18}FN_7NaO_3$ $[M + Na]^+$ 434.1347, found 434.1338.

1-(4-(1*H*-pyrazolo[3,4-*d*]pyrimidin-4-yloxy)-3-chlorophenyl)-3-(5-tert-butyli soxazol-3-yl)urea (18c) The title compound was synthesized in a manner similar to the synthesis of **7a** using compounds **17c** and **4a** to give compound **18c**, which was purified by column chromatography (eluent gradient petroleum ether:EtOAc, 3:1) and recrystallized from EtOAc and petroleum ether. Yield: 96%, 100% HPLC purity. ^{1}H NMR(400 MHz, DMSO-d_6): δ 14.23 (s, 1H), 9.67 (s, 1H), 9.10 (s, 1H), 8.52 (s, 1H), 8.26 (s, 1H), 7.89 (d, *J*=2.0 Hz, 1H), 7.46-7.41 (m, 2H), 6.52 (s, 1H), 1.30 (s, 9H) ppm; δ 180.8, 162.7, 158.7, 157.3, 155.3, 151.9, 143.0, 138.6, 132.2, 125.6, 125.0, 120.1, 119.1, 101.5, 93.0, 33.0, 28.8, 16.4 ppm; HRMS (m/z): calcd for $C_{19}H_{19}ClN_7O_3$ $[M + H]^+$ 428.1232, found 428.1223; $C_{19}H_{18}ClN_7NaO_3$ $[M + Na]^+$ 450.1052, found 450.1051.

1-(4-(1*H*-pyrazolo[3,4-*d*]pyrimidin-4-yloxy)-3-methylphenyl)-3-(3-tert-butyl-1-methyl-1*H*-pyrazol-5-yl)urea (18e) The title compound was synthesized in a

manner similar to the synthesis of **7a** using compounds **17e** and **4a** to give **18e**, which was purified by column chromatography (eluent gradient petroleum ether:EtOAc, 2:1) and recrystallized from EtOAc and petroleum ether. Yield: 57%, 96.8% HPLC purity. ^{1}H NMR (400 MHz, DMSO-d_6): δ 14.14 (s, 1H), 9.54 (s, 1H), 8.86 (s, 1H), 8.49 (s, 1H), 8.00 (s, 1H), 7.48 (s, 1H), 7.36 (d, *J*=8.8 Hz, 1H), 7.18 (d, *J*=8.8 Hz, 1H), 6.52 (s, 1H), 2.07 (s, 3H), 1.30 (s, 9H) ppm; ^{13}C NMR (100 MHz, DMSO-d_6): δ 180.7, 163.3, 158.9, 157.3, 155.5, 151.9, 146.1, 137.4, 132.2, 131.1, 123.1, 121.6, 118.0, 101.6, 92.9, 33.0, 28.8, 16.4 ppm; HRMS (m/z): calcd for $C_{20}H_{22}N_7O_2$ $[M + H]^+$ 408.1779, found 408.1760; $C_{20}H_{21}N_7NaO_2$ $[M + Na]^+$ 430.1598, found 430.1581.

1-(4-(1*H*-pyrazolo[3,4-*d*]pyrimidin-4-yloxy)-3-fluorophenyl)-3-(3-tert-butyl-1-phenyl-1*H*-pyrazol-5-yl)urea (19b) The title compound was synthesized in a manner similar to the synthesis of **7a** using compounds **17b** and **8d** to give compound **19b**, which was purified by column chromatography (eluent gradient CH_2Cl_2:MeOH, 60:1) and recrystallized from EtOAc and petroleum ether.Yield: 86%, 98.3% HPLC purity. ^{1}H NMR (400 MHz, DMSO-d_6): δ 14.22 (s, 1H), 9.31 (s, 1H), 8.53 (s, 1H), 8.50 (s, 1H), 8.30 (s, 1H), 7.66 (d, *J*=2.4 Hz, 1H), 7.55 (d, *J*=4.4 Hz 4H), 7.43-7.39 (m, 2H), 7.21 (d, *J*=2.4 Hz, 1H), 6.40 (s, 1H), 1.29(s, 9H) ppm; ^{13}C NMR (100 MHz, DMSO-d_6): δ 170.3, 162.2, 160.8, 156.7, 154.8, 151.7, 142.1, 138.6, 136.8, 131.7, 129.3, 127.4, 126.0, 124.5, 124.2, 119.2, 118.1, 101.0, 96.1, 32.0, 30.1 ppm; LC-MS m/z: 487.2 $[M + H]^+$.

1-(4-(1*H*-pyrazolo[3,4-*d*]pyrimidin-4-yloxy)-3-fluorophenyl)-3-(3-tert-butyl-1-cyclopentyl-1*H*-pyrazol-5-yl)urea (19c) The title compound was synthesized in a

manner similar to the synthesis of **7a** using compounds **17b** and **8b** to give compound **19c**, which was purified by column chromatography (eluent gradient CH_2Cl_2:MeOH, 65:1) and recrystallized from EtOAc and petroleum ether. Yield: 94%, 98.2% HPLC purity. ^{1}H NMR (400 MHz, DMSO-d_6): δ 14.24 (s, 1H), 9.16 (s, 1H), 8.52 (s, 1H), 8.49 (s, 1H), 8.30 (s, 1H), 7.68 (dd, *J*=2.4 Hz, *J*=10.8 Hz, 1H), 7.40 (t, *J*=8.8 Hz, 1H), 7.24 (d, *J*=8.8 Hz, 1H), 6.05 (s, 1H), 4.55-4.48 (m, 1H), 1.98-1.89 (m, 4H), 1.88-1.80 (m, 2H), 1.62-1.56 (m, 2H), 1.22 (s, 9H) ppm; ^{13}C NMR (100 MHz, DMSO-d_6): δ 162.6, 158.9, 157.2, 155.3, 152.8, 152.6, 139.5, 135.3, 133.5, 132.2, 124.7, 114.9, 107.0, 101.4, 95.2, 57.5, 32.4, 30.9, 24.4 ppm; HRMS (m/z): calcd for $C_{24}H_{28}FN_8O_2$ $[M + H]^+$ 479.2314, found 4179.2314; $C_{24}H_{27}FN_8NaO_2$ $[M + Na]^+$ 501.2135, found 501.21338.

The synthetic methods and characterization data for other target compounds reported in this study are given in Supporting Information. The ^{1}H NMR, ^{13}C NMR, HRMS spectra and HPLC chromatograms of the target compounds are also shown in Supporting Information Figure S1-S26.

Kinase Inhibitory Assays

The kinase inhibitory assays were performed according to the KinaseProfiler assay protocols of Eurofins Pharma Discovery Services UK Limited (Eurofins).

K14-VEGF Transgenic Mice

The K14-VEGF transgenic homozygous mice were purchased from Jackson Laboratories (Bar Harbor, ME, USA). The high expression of VEGF in the skin tissue could induce inflammatory skin condition with similar characteristics of psoriasis,

including erythematous and scaly skin, moderate acanthosis, parakeratosis, hyperplastic inflamed blood vessels, and typical inflammatory cell infiltrate.

In the experiments, 3- to 4-month-old K14-VEGF mice with moderate to serious psoriasis were chosen and re-derived to homozygosity. The same batch of K14-VEGF transgenic homozygous mice were divided into two groups as follows: treatment group receiving compound **18b** and control groups receiving only vehicle. Mice were smeared with cream contained 0.05% compound **18b** or not on psoriatic lesions for 3 weeks. After the final treatment, the mice were housed and observed for another 15 days. Photographs of mouse head and neck were obtained at day 0, 21 and 36. All animal experiments described in this study were approved by the Institutional Animal Care and Use Committee of Sichuan University.

pDC and mDC Cultures

Balb/c mice were kept under SPF conditions. To generate pDCs and mDCs, femurs and tibias of mice were removed and purified as described previously.[45,46] Then, BM cells were flushed with PBS using a syringe with a 0.45 mm diameter needle. Whole BM cells (1×10^6/ml) were cultured in 6-well plates in RPMI-1640 medium supplemented with 10% FCS, 10^{-4} M 2-ME (Sigma-Aldrich), sodium pyruvate (Gibco), 100 μg/ml penicillin (Sigma-Aldrich), 100 μg/ml streptomycin (Sigma-Aldrich) and 100 ng/ml FLT3L (Peprotech) as indicated for 9 days.

Elisa

pDCs and mDCs were induced for 9 days as mentioned before. On day 9, compound **18b** with indicated concentrations dissolved in DMSO was added in the

culture medium. After 12 h, the content of IFN-γ and IL-23 in the culture medium was analysed by Elisa following the manufacture instructions.

K14-VEGF mice were treated with compound **18b** (n=3) or vehicle (n=3) for 29 days as mentioned before. At termination, blood samples were collected as described previously and kept in 4 ℃ for 12 h. After centrifugation, the content of IFN-γ and IL-17 in plasma was quantified by Elisa according to the manufacturer's protocol.

Flow Cytometric Analysis

pDCs and mDCs were induced for 9 days as mentioned before. On day 9, indicated concentration of compound **18b** dissolved in DMSO was added in the culture medium. After 24 h, cells were incubated with antibodies against CD11c PerCP, CD45R/B220 FITC or I-A/I-E (MHC class II) FITC for 30 min and analysed by flow cytometric as indicated.[47] pDCs were identified as $CD11c^+$ $B220^+$ and mDCs as $CD11c^+$ MHC class II^+ cells.

The cells in the skin tissue sections and lymph nodes were harvested as indicated before. For the skin section cells detection, three- or two-color staining was performed using mouse anti-FLT3 PE, anti-CD11c PerCP, anti-B220 FITC, and I-A/I-E FITC antibodies. For the lymphocyte detection, cells were first surface-stained with anti-CD4 PE followed by fixing and permeabilisation. After the permeabilisation, the FITC-labeled anti-mouse IL-17 antibody was added.

All the antibodies were obtained from Becton-Dickinson. Cells were analysed using a flow cytometer (Becton-Dickinson), and data were processed using FlowJo software.

Western Blot Analysis

BMDCs were cultured as above. On day 9, compound **18b** was added to the culture medium for 1 h. Cells were harvested and subjected to western blot analysis with rabbit anti-mouse STAT3, STAT5, pSTAT3 and pSTAT5 antibodies as previously described.[27] All the antibodies were purchased from Abcam.

Histology

K14-VEGF mice were treated with compound **18b** (n=3) or vehicle (n=3) for 29 days as mentioned before. The skin lesion sections were collected and embedded in paraffin. Then the HE and immunohistochemistry assays were performed as indicated.[48] The positive areas were assessed using the Imagepro Plus software. All the antibodies were purchased from Cell Signaling Technology.

Associated Content

Supporting Information

The Supporting Information is available free of charge on the ACS Publications website at DOI: 00.0000/acs.jmedchem.0000000.

Supplementary methods section giving the synthetic methods and characterization data for the target compounds that are not included in the main text; Figure S1-S26 showing ^{1}H NMR, ^{13}C NMR, HRMS spectra and HPLC chromatograms of the target compounds. Molecular formula strings of the target compounds were uploaded as "Molecular Formula Strings.csv".

Corresponding Authors

*Phone: +86-28-85164063. E-mail: yangsy@scu.edu.cn.

Author Contributions

[#]G.B. Li and S. Ma contributed equally to this work.

Notes

The authors declare no competing financial interest.

Acknowledgements

This work was supported by the 973 Program (2013CB967204), the National Natural Science Foundation of China (81325021, 81473140, 81573349), and the Program for Changjiang Scholars and Innovative Research Team in University (IRT13031).

Abbreviations Used

SAR, structure-activity relationship; DCs, dendritic cells; FLT3, FMS-like tyrosine kinase 3; FLT3L, FLT3 ligand; IL, interleukin; TGF, transforming growth factor; IFN, interferon; VEGF, vascular endothelial growth factor; pDCs, plasmacytoid DCs; mDCs, myeloidDCs; BMDCs, bone marrow-derived cells; STAT, signal transducer and activator of transcription; pSTAT, phosphorylated STAT; DMF, *N*,*N*-dimethylformamide; TLC, thin layer chromatography; TMS, tetramethylsilane; ESI, electrospray ionization.

References

(1) Nestle, F. O.; Kaplan, D. H.; Barker, J. Psoriasis. *N. Engl. J. Med.* **2009**, *361*, 496-509.

(2) Ryan, C.; Abramson, A.; Patel, M.; Menter, A. Current investigational drugs in psoriasis. *Expert. Opin. Inv. Drug.* **2012**, *21*, 473-487.

(3) Lowes, M. A.; Bowcock, A. M.; Krueger, J. G. Pathogenesis and therapy of

psoriasis. *Nature* **2007**, *445*, 866-873.

(4) Whartenby, K. A.; Small, D.; Calabresi, P. A. FLT3 inhibitors for the treatment of autoimmune disease. *Expert. Opin. Inv. Drug.* **2008**, *17*, 1685-1692.

(5) Jariwala, S. P. The role of dendritic cells in the immunopathogenesis of psoriasis. *Arch. Dermatol. Res.* **2007**, *299*, 359-366.

(6) Khandpur, S.; Bhari, N. Newer targeted therapies in psoriasis. *Indian J. Dermatol. Venereol. Leprol.* **2013**, *79*, S47-S52.

(7) Novelli, L.; Chimenti, M. S.; Chiricozzi, A.; Perricone, R. The new era for the treatment of psoriasis and psoriatic arthritis: Perspectives and validated strategies. *Autoimmun. Rev.* **2014**, *13*, 64-69.

(8) Feely, M. A.; Smith, B. L.; Weinberg, J. M. Novel psoriasis therapies and patient outcomes, part 2: biologic treatments. *Cutis* **2015**, *95*, 282-290.

(9) Lee, H. J.; Li, C. W.; Hammerstad, S. S.; Stefan, M.; Tomer, Y. Immunogenetics of autoimmune thyroid diseases: A comprehensive review. *J. Autoimmun.* **2015**, *64*, 82-90.

(10) Nagy, G.; Huszthy, P. C.; Fossum, E.; Konttinen, Y.; Nakken, B.; Szodoray, P. Selected aspects in the pathogenesis of autoimmune diseases. *Mediators Inflamm.* **2015**, *2015*, 351732.

(11) Thomas, R. Dendritic cells as targets or therapeutics in rheumatic autoimmune disease. *Curr. Opin. Rheumatol.* **2014**, *26*, 211-218.

(12) Mann, E. R.; Li, X. H. Intestinal antigen-presenting cells in mucosal immune homeostasis: Crosstalk between dendritic cells, macrophages and B-cells. *World J. Gastroenterol.* **2014**, *20*, 9653-9664.

(13) Makala, L. H. C.; Nagasawa, H. Dendritic cells: A specialized complex system of antigen presenting cells. *J. Vet. Med. Sci.* **2002**, *64*, 181-193.

(14) Glitzner, E.; Korosec, A.; Brunner, P. M.; Drobits, B.; Amberg, N.; Schonthaler, H. B.; Kopp, T.; Wagner, E. F.; Stingl, G.; Holcmann, M.; Sibilia, M. Specific roles for dendritic cell subsets during initiation and progression of psoriasis. *Embo Mol. Med.* **2014**, *6*, 1312-1327.

(15) Banchereau, J.; Steinman, R. M. Dendritic cells and the control of immunity.

Nature **1998**, *392*, 245-252.

(16) Mellman, I.; Steinman, R. M. Dendritic cells: specialized and regulated antigen processing machines. *Cell* **2001**, *106*, 255-258.

(17) Guttman-Yassky, E.; Lowes, M. A.; Fuentes-Duculan, J.; Zaba, L. C.; Cardinale, I.; Nograles, K. E.; Khatcherian, A.; Novitskaya, I.; Carucci, J. A.; Bergman, R.; Krueger, J. G. Low expression of the IL-23/Th17 pathway in atopic dermatitis compared to psoriasis. *J. Immunol.* **2008**, *181*, 7420-7427.

(18) Huh, J. R.; Leung, M. W. L.; Huang, P.; Ryan, D. A.; Krout, M. R.; Malapaka, R. R. V.; Chow, J.; Manel, N.; Ciofani, M.; Kim, S. V.; Cuesta, A.; Santori, F. R.; Lafaille, J. J.; Xu, H. E.; Gin, D. Y.; Rastinejad, F.; Littman, D. R. Digoxin and its derivatives suppress Th17 cell differentiation by antagonizing RORγt activity. *Nature* **2011**, *472*, 486-490.

(19) Ramos, M. I.; Tak, P. P.; Lebre, M. C. Fms-like tyrosine kinase 3 ligand-dependent dendritic cells in autoimmune inflammation. *Autoimmun. Rev.* **2014**, *13*, 117-124.

(20) D'Amico, A.; Wu, L. The early progenitors of mouse dendritic cells and plasmacytoid predendritic cells are within the bone marrow hemopoietic precursors expressing Flt3. *J. Exp. Med.* **2003**, *198*, 293-303.

(21) Karsunky, H.; Merad, M.; Cozzio, A.; Weissman, I. L.; Manz, M. G. Flt3 ligand regulates dendritic cell development from Flt3+ lymphoid and myeloid-committed progenitors to Flt3+ dendritic cells in vivo. *J. Exp. Med.* **2003**, *198*, 305-313.

(22) Brasel, K.; De Smedt, T.; Smith, J. L.; Maliszewski, C. R. Generation of murine dendritic cells from flt3-ligand–supplemented bone marrow cultures. *Blood* **2000**, *96*, 3029-3039.

(23) Pulendran, B.; Lingappa, J.; Kennedy, M. K.; Smith, J.; Teepe, M.; Rudensky, A.; Maliszewski, C. R.; Maraskovsky, E. Developmental pathways of dendritic cells in vivo: distinct function, phenotype, and localization of dendritic cell subsets in FLT3 ligand-treated mice. *J. Immunol.* **1997**, *159*, 2222-2231.

(24) Ding, Y. T.; Wilkinson, A.; Idris, A.; Fancke, B.; O'Keeffe, M.; Khalil, D.; Ju, X. S.; Lahoud, M. H.; Caminschi, I.; Shortman, K.; Rodwell, R.; Vuckovic, S.; Radford,

K. J. FLT3-ligand treatment of humanized mice results in the generation of large numbers of CD141(+) and CD1c(+) dendritic cells *in vivo*. *J. Immunol.* **2014**, *192*, 1982-1989.

(25) Karsunky, H.; Merad, M.; Cozzio, A.; Weissman, I. L.; Manz, M. G. Flt3 ligand regulates dendritic cell development from Flt3(+) lymphoid and myeloid-committed progenitors to Flt3(+) dendritic cells *in vivo*. *J. Exp. Med.* **2003**, *198*, 305-313.

(26) Whartenby, K. A.; Calabresi, P. A.; McCadden, E.; Nguyen, B.; Kardian, D.; Wang, T.; Mosse, C.; Pardoll, D. M.; Small, D. Inhibition of FLT3 signaling targets DCs to ameliorate autoimmune disease. *Proc. Natl. Acad. Sci. U.S.A.* **2005**, *102*, 16741-16746.

(27) Yan, H.-X.; Li, W.-W.; Zhang, Y.; Wei, X.-W.; Fu, L.-X.; Shen, G.-B.; Yin, T.; Li, X.-Y.; Shi, H.-S.; Wan, Y.; Zhang, Q.-Y.; Li, J.; Yang, S.-Y.; Wei, Y.-Q. Accumulation of FLT3+ CD11c+ dendritic cells in psoriatic lesions and the anti-psoriatic effect of a selective FLT3 inhibitor. *Immunol. Res.* **2014**, *60*, 112-126.

(28) Yang, L.-L.; Li, G.-B.; Ma, S.; Zou, C.; Zhou, S.; Sun, Q.-Z.; Cheng, C.; Chen, X.; Wang, L.-J.; Feng, S. Structure–activity relationship studies of pyrazolo [3, 4-d] pyrimidine derivatives leading to the discovery of a novel multikinase inhibitor that potently inhibits FLT3 and VEGFR2 and evaluation of its activity against acute myeloid leukemia *in vitro* and *in vivo*. *J. Med. Chem.* **2013**, *56*, 1641-1655.

(29) Xia, Y. P.; Li, B.; Hylton, D.; Detmar, M.; Yancopoulos, G. D.; Rudge, J. S. Transgenic delivery of VEGF to mouse skin leads to an inflammatory condition resembling human psoriasis. *Blood* **2003**, *102*, 161-168.

(30) Hvid, H.; Teige, I.; Kvist, P. H.; Svensson, L.; Kemp, K. TPA induction leads to a Th17-like response in transgenic K14/VEGF mice: a novel *in vivo* screening model of psoriasis. *Int. Immunol.* **2008**, *20*, 1097-1106.

(31) Wang, X. G.; Sun, J.; Hu, J. H. IMQ induced K14-VEGF mouse: a stable and long-term mouse model of psoriasis-like inflammation. *Plos One* **2015**, *10*, e0145498.

(32) Hvid, H.; Svensson, L.; Kvist, P. H.; Kemp, K.; Petersen, T. K. A psoriasis-like cutaneous inflammation in K14/VEGF-transgenic mice is characterised by epidermal hyperplasia and pronounced infiltration of T-cells in the skin. *Inflamm. Res.* **2007**, *56*,

S437-S438.

(33) Yang, L. L.; Li, G. B.; Yan, H. X.; Sun, Q. Z.; Ma, S.; Ji, P.; Wang, Z. R.; Feng, S.; Zou, J.; Yang, S. Y. Discovery of N6-phenyl-1*H*-pyrazolo[3,4-*d*]pyrimidine-3,6-diamine derivatives as novel CK1 inhibitors using common-feature pharmacophore model based virtual screening and hit-to-lead optimization. *Eur. J. Med. Chem.* **2012**, *56*, 30-38.

(34) Ranatunge, R. R.; Augustyniak, M.; Bandarage, U. K.; Earl, R. A.; Ellis, J. L.; Garvey, D. S.; Janero, D. R.; Letts, L. G.; Martino, A. M.; Murty, M. G.; Richardson, S. K.; Schroeder, J. D.; Shumway, M. J.; Tam, S. W.; Trocha, A. M.; Young, D. V. Synthesis and selective cyclooxygenase-2 inhibitory activity of a series of novel, nitric oxide donor-containing pyrazoles. *J. Med. Chem.* **2004**, *47*, 2180-2193.

(35) Lutz, M. B.; Kukutsch, N.; Ogilvie, A. L. J.; Rößner, S.; Koch, F.; Romani, N.; Schuler, G. An advanced culture method for generating large quantities of highly pure dendritic cells from mouse bone marrow. *J. Immunol. Methods* **1999**, *223*, 77-92.

(36) Nestle, F. O.; Conrad, C.; Tun-Kyi, A.; Homey, B.; Gombert, M.; Boyman, O.; Burg, G.; Liu, Y. J.; Gilliet, M. Plasmacytoid predendritic cells initiate psoriasis through interferon-alpha production. *J. Exp. Med.* **2005**, *202*, 135-143.

(37) Lee, E.; Trepicchio, W. L.; Oestreicher, J. L.; Pittman, D.; Wang, F.; Chamian, F.; Dhodapkar, M.; Krueger, J. G. Increased expression of interleukin 23 p19 and p40 in lesional skin of patients with psoriasis vulgaris. *J. Exp. Med.* **2004**, *199*, 125-130.

(38) Sabat, R.; Philipp, S.; Hoeflich, C.; Kreutzer, S.; Wallace, E.; Asadullah, K.; Volk, H. D.; Sterry, W.; Wolk, K. Immunopathogenesis of psoriasis. *Exp. Dermatol.* **2007**, *16*, 779-798.

(39) Kieslinger, M.; Woldman, I.; Moriggl, R.; Hofmann, J.; Marine, J.-C.; Ihle, J. N.; Beug, H.; Decker, T. Antiapoptotic activity of Stat5 required during terminal stages of myeloid differentiation. *Genes Dev.* **2000**, *14*, 232-244.

(40) Laouar, Y.; Welte, T.; Fu, X.-Y.; Flavell, R. A. STAT3 is required for Flt3L-dependent dendritic cell differentiation. *Immunity* **2003**, *19*, 903-912.

(41) Zhang, W.-y.; Wang, Y.; Guo, Y.-l.; Dai, H.-r.; Yang, Q.-m.; Zhang, Y.-j.; Zhang, Y.; Chen, M.-x.; Wang, C.-m.; Feng, K.-c.; Li, S.-x.; Liu, Y.; Shi, F.-x.; Luo, C.; Han,

W.-d. Treatment of CD20-directed Chimeric Antigen Receptor-modified T cells in patients with relapsed or refractory B-cell non-Hodgkin lymphoma: an early phase IIa trial report. *Signal Transduct. Target. Ther.* **2016**, *1*, 16002.

(42) Singh, T. P.; Schon, M. P.; Wallbrecht, K.; Michaelis, K.; Rinner, B.; Mayer, G.; Schmidbauer, U.; Strohmaier, H.; Wang, X. J.; Wolf, P. 8-methoxypsoralen plus ultraviolet A therapy acts via inhibition of the IL-23/Th17 axis and induction of Foxp3+ regulatory T cells involving CTLA4 signaling in a psoriasis-like skin disorder. *J. Immunol.* **2010**, *184*, 7257-7267.

(43) Haider, A. S.; Lowes, M. A.; Suárez-Fariñas, M.; Zaba, L. C.; Cardinale, I.; Khatcherian, A.; Novitskaya, I.; Wittkowski, K. M.; Krueger, J. G. Identification of cellular pathways of "type 1," Th17 T cells, and TNF- and inducible nitric oxide synthase-producing dendritic cells in autoimmune inflammation through pharmacogenomic study of cyclosporine A in psoriasis. *J. Immunol.* **2008**, *180*, 1913-1920.

(44) Fitch, E. L.; Rizzo, H. L.; Kurtz, S. E.; Wegmann, K. W.; Gao, W.; Benson, J. M.; Hinrichs, D. J.; Blauvelt, A. Inflammatory skin disease in K5.hTGF-β1 transgenic mice is not dependent on the IL-23/Th17 inflammatory pathway. *J. Invest. Dermatol.* **2009**, *129*, 2443-2450.

(45) Tussiwand, R.; Onai, N.; Mazzucchelli, L.; Manz, M. G. Inhibition of natural type I IFN-producing and dendritic cell development by a small molecule receptor tyrosine kinase inhibitor with Flt3 affinity. *J. Immunol.* **2005**, *175*, 3674-3680.

(46) Lutz, M. B.; Kukutsch, N.; Ogilvie, A. L. J.; Rossner, S.; Koch, F.; Romani, N.; Schuler, G. An advanced culture method for generating large quantities of highly pure dendritic cells from mouse bone marrow. *J. Immunol. Methods* **1999**, *223*, 77-92.

(47) Shen, W.; Du, R.; Li, J.; Luo, X.; Zhao, S.; Chang, A.; Zhou, W.; Gao, R.; Luo, D.; Wang, J.; Hao, N.; Liu, Y.; Chen, Y.; Luo, Y.; Sun, P.; Yang, S.; Luo, N.; Xiang, R. TIFA suppresses hepatocellular carcinoma progression via MALT1-dependent and -independent signaling pathways. *Signal Transduct. Target. Ther.* **2016**, *1*, 16013.

(48) Wert, K. J.; Mahajan, V. B.; Zhang, L.; Yan, Y.; Li, Y.; Tosi, J.; Wei Hsu, C.; Nagasaki, T.; Janisch, K. M.; Grant, M. B.; Mahajan, M.; Bassuk, A. G.; Tsang, S. H.

Neuroretinal hypoxic signaling in a new preclinical murine model for proliferative diabetic retinopathy. *Signal Transduct. Target. Ther.* **2016**, *1*, 16005.

Scheme 1 [a]

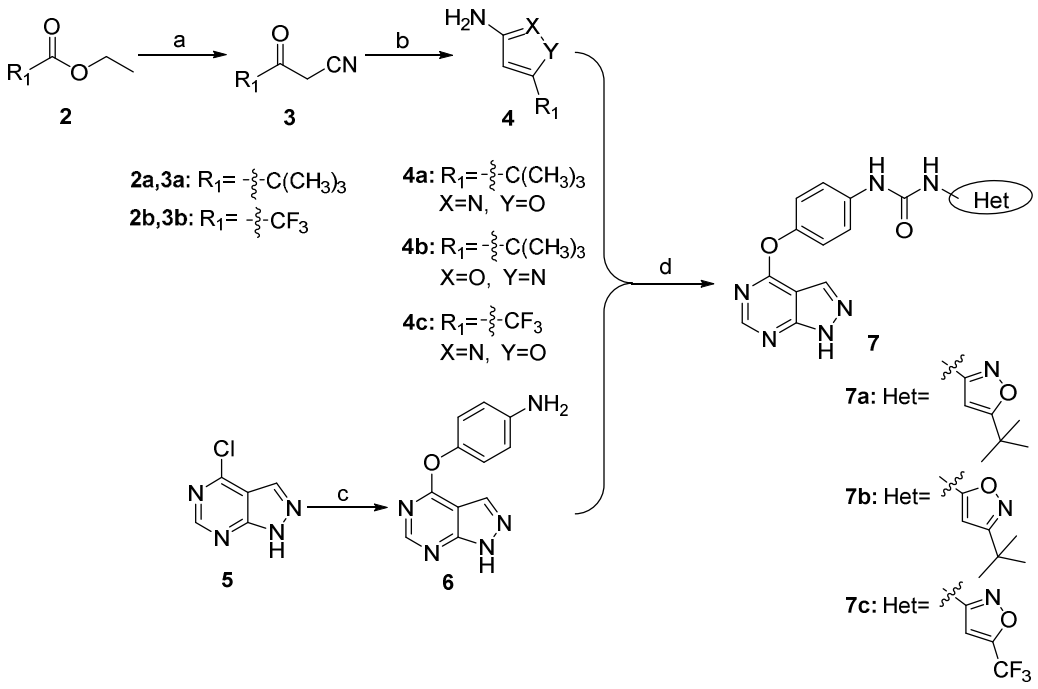

[a]Reagents and conditions: (a) acetonitrile, NaH, THF, 80 ℃, 68%-84%; (b) for **4a**, **4c**:hydroxylamine hydrochloride NaOH, H_2O, HCl, RT-55 ℃, 24%-61%; for **4b**:hydroxylamine hydrochloride, NaOH,H_2O, 100 ℃, 66%; (c) 4-aminophenol, NaOH, H_2O, THF, 60 ℃, 32%; (d) triphosgene, THF, Et_3N, RT-reflux, 2-8h; **6**, acetonitrile, toluene, 110 ℃, 16 h, 58%-89%.

Scheme 2 [a]

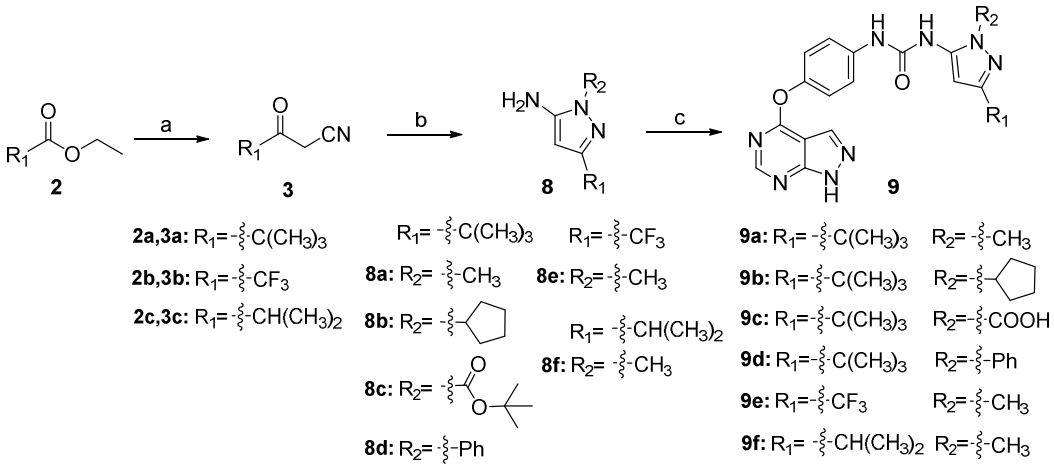

[a] Reagents and conditions: (a) acetonitrile, NaH, THF, 80 ℃, 68%-84%; (b) R_2NHNH_2, EtOH, 90 ℃, 55%-84%; (c) triphosgene, THF, Et_3N, RT-reflux, 2-12h; acetonitrile, toluene, 110 ℃, 58%-92%.

Scheme 3 [a]

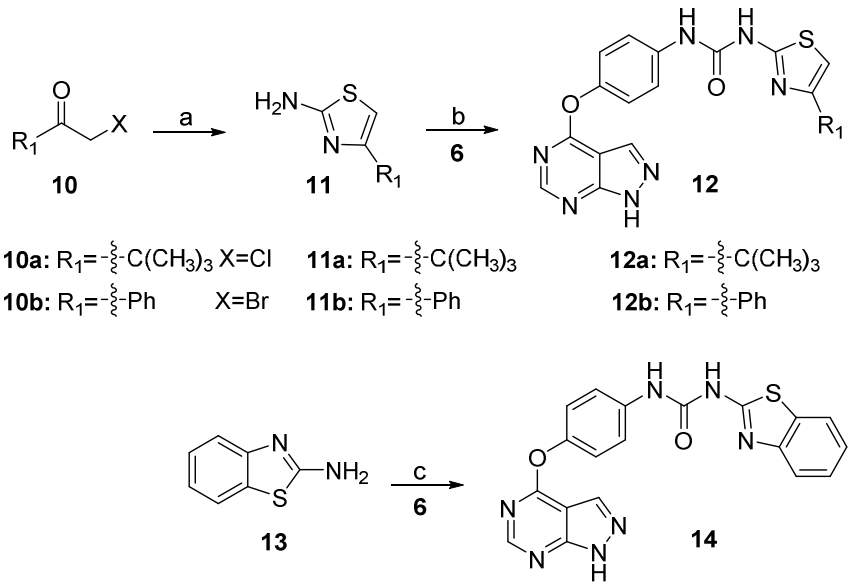

[a] Reagents and conditions: (a) thiocarbamide, EtOH, 90 ℃, 75%-88%; (b) triphosgene, THF, Et_3N, RT-reflux, 4-8h; acetonitrile, toluene, 110 ℃, 16 h, 71%-76%; (c) triphosgene, toluene, Et_3N, 60 ℃-reflux, 12h; **6**, toluene, 120 ℃, 16 h, 43%.

Scheme 4 [a]

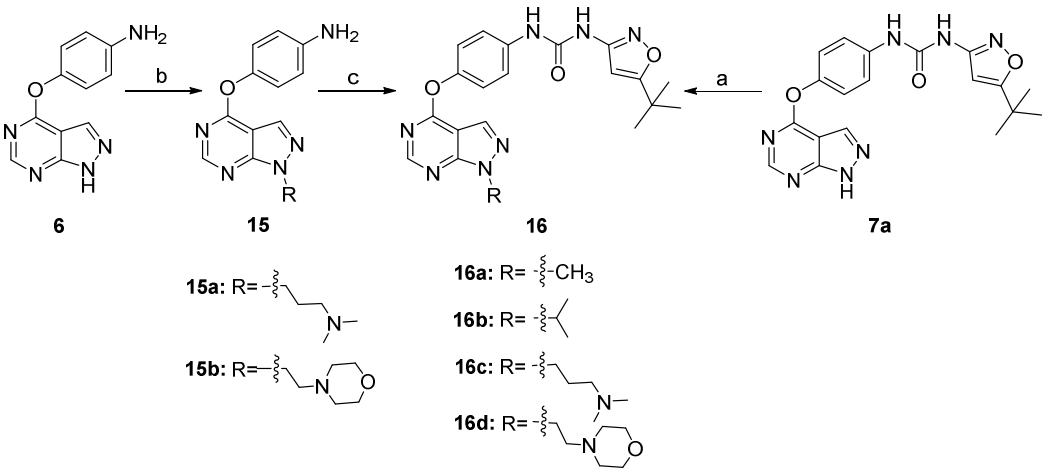

[a] Reagents and conditions: (a) RX, NaOH, DMF, 61%-94%; (b) RX, NaOH, K_2CO_3, DMF, RT-100 ℃, 4 h, 84%-90%; (c) for **16c**, **16d**: acetonitrile, toluene, 110 ℃, 16 h, 74%-76%.

Scheme 5[a]

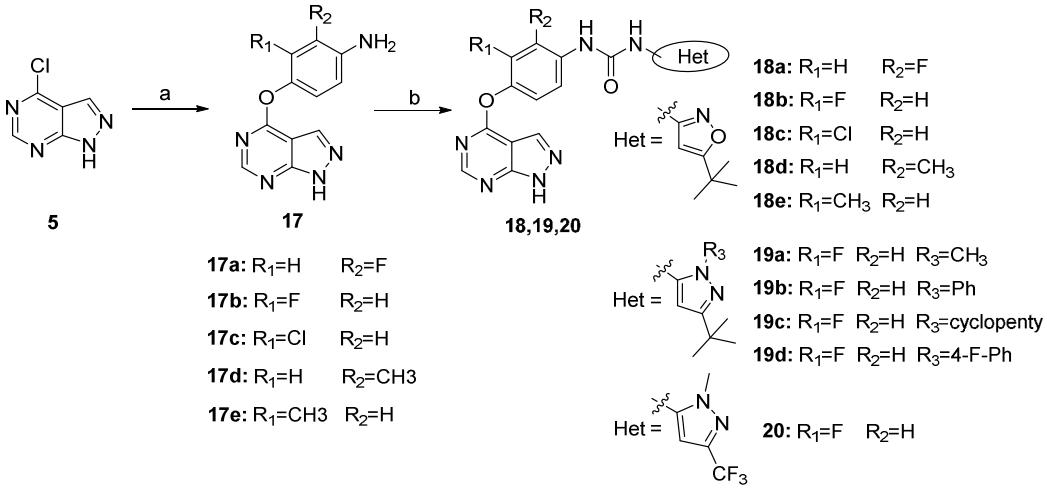

[a] Reagents and conditions: (a) aminophenols, sodium hydroxide, H_2O, THF, RT-60 ℃, 41%-66%; (b) for **18a-18e**: isocyanates, acetonitrile, toluene, 110 ℃, 16 h, 51%-96%; for **19a-19d**, **20**: **17b**, triphosgene, triethylamine, acetonitrile, toluene, 120 ℃, 16 h, 56%-94%.

Table1.1-(4-(1*H*-Pyrazolo[3,4-*d*]pyrimidin-4-yloxy)phenyl)urea derivatives containing various substitutions (R) at 3-*N* of urea and their inhibitory activities against FLT3.

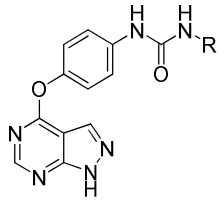

Cpd	R	FLT3[a](IC$_{50}$, nM)	Cpd	R	FLT3[a](IC$_{50}$, nM)
1	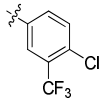	39± 4.2	**9d**	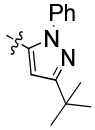	50 ± 6.6
7a	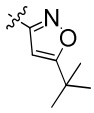	11 ± 1.2	**9e**	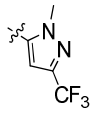	38 ± 4.2
7b		8 ± 0.9	**9f**	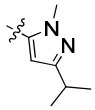	82 ± 9.0
7c		28 ± 3.3	**12a**		8 ± 1.5
9a	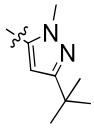	62 ± 6.9	**12b**		73 ± 9.0
9b	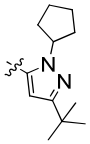	52± 6.0	**14**	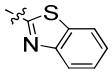	294 ± 32.4
9c	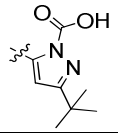	10 ± 1.2			

[a]Each compound was tested in triplicate; the data are presented as the mean ± SD.

Table 2. 1-(4-(1*H*-pyrazolo[3,4-*d*]pyrimidine-4-yloxy)phenyl)urea derivatives with different substituents at *N*-1 position (R) of the pyrazolo[3,4-*d*]pyrimidine and their inhibitory activities against FLT3.

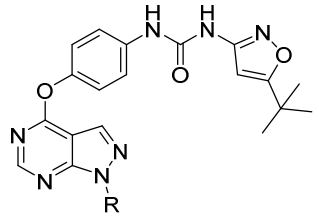

Cpd	R	FLT3[a](IC$_{50}$, nM)
7a	H	11 ± 1.2
16a		27 ± 3.6
16b		217 ± 32.1
16c	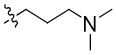	80 ± 9.6
16d	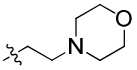	449 ± 52.8

[a]Each compound was tested in triplicate; the data are presented as the mean ± SD.

Table 3. 1-(4-(1*H*-Pyrazolo[3,4-*d*]pyrimidin-4-yloxy)phenyl)urea derivatives containing various substituents at the benzene ring (R_1, R_2) and 3-position of urea (R_3) and their inhibitory activities against FLT3.

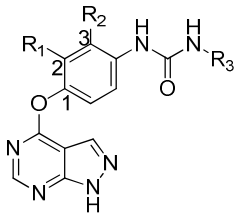

Cpd	R_1	R_2	R_3	FLT3[a] (IC_{50}, nM)
18a	H	F	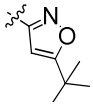	6± 0.9
18b	F	H		5± 0.6
18c	Cl	H		2± 0.3
18d	H	CH_3		657± 72.6
18e	CH_3	H	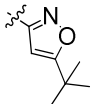	6± 0.8
19a	F	H	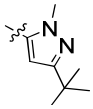	66± 10.2
19b	F	H	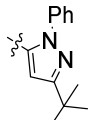	56± 8.4
19c	F	H	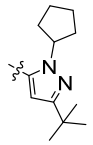	53± 6.9
19d	F	H	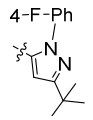	42± 5.7
20	F	H	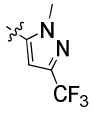	36 ± 4.2

[a]Each compound was tested in triplicate; the data are presented as the mean ± SD.

Figure captions:

Figure 1. (a) Structure of compound **1**. (b) Schematic showing subgroups or atoms that were the focus of structural modifications.

Figure 2. Compound **18b** showed considerable abilities to suppress the generation of DCs from BMDCs and inhibit cytokine secretion of DCs through the blockade of FLT3 signaling pathway *in vitro*. BM cells flushed from the femurs and tibias of BALB/c mice were cultured in RPMI 1640 medium supplemented with 10% FCS, 10^{-4} M 2-ME, sodium pyruvate, antibiotics, 100 nM FLT3L for 9 days. On 9^{th} day, compound **18b** or 0.1% DMSO was added to the culture medium for 24 h (a), 12 h (b) and 1 h (c), followed by flow cytometric, Elisa and western blot assays as indicated. (a) Flow cytometric analysis of the $CD11c^+$ $B220^+$ cells (pDCs) or the $CD11c^+$ MHC II^+ cells (mDCs). Representative flow cytometric analyses are shown; (b) IFN-γ and IL-23 in the supernatant were analyzed and quantified by Elisa; (c) Whole BM cells were lysed to evaluate the phosphorylation state of STAT3 and STAT5 by western blot. All the histogram shows the statistics data of three independent experiments.

Figure 3. Anti-psoriatic activity of compound **18b** on K14-VEGF transgenic mice. K14-VEGF transgenic mice were treated as indicated in materials and methods section. (a) Macroscopic images of the mice after treatment with vehicle (left), compound **18b** (middle) and the mice 15 days after the last administration of compound **18b** (right); (b) HE staining of head and neck tissue sections after the treatment of compound **18b** for 29 days; (c) Quantitative assessments of the pathological score, based on the Baker score system, were performed in 5 randomly chosen fields. Mean scores and SD values are shown; (d) Epidermal thickness were measured in 8 randomly chosen fields (mean ± SEM).

Figure 4. Flow cytometric quantification of $FLT3^+$ $CD11c^+$ DCs in single-cell suspensions isolated from vehicle-treated and compound **18b**-treated psoriatic plaque lesions. (a) Representative flow cytometric analyses of $FLT3^+$ $CD11c^+$ DCs are shown. (b) $FLT3^+$ cells were first gated and then plotted as CD11c versus B220 or

MHC class II. Ordinates in the histogram indicate the percentage of each cell type within total skin cells. Data are representative of three independent experiments.

Figure 5. Immunohistochemical staining of tissue sections after treatments in a pharmacodynamic experiment. K14-VEGF transgenic mice were treated as indicated in Materials and Methods. After treatment 29 days, mice were killed, and 4-μm-thick paraffin-embedded ear skin sections were stained by immunohistochemistry to detect T lymphocyte infiltrationand related chemokines and growth factors in vehicle-treated and compound **18b**-treated mice. Quantitative immunohistochemical analysis were processed using the Imagepro Plus software in 5 randomly chosen fields and the data are shown in the histogram (mean ± SD, n=5 per group).

Figure 6. Inhibition of Th17/Th1 cells by compound **18b** treatment *in vivo*. Psoriasis model mice were treated with compound **18b** or vehicle for 29 days. (a) The lymph nodes were analysed by flow cytometry for Th17 cells ($CD4^+$ $IL\text{-}17^+$ cells). Data (mean ± SD) are representative of independent experiments using three mice; (b) The blood plasma was used for Elisa analysis of IL-17 and IFN-γ. Data (mean ± SD) are representative of independent experiments using three mice.

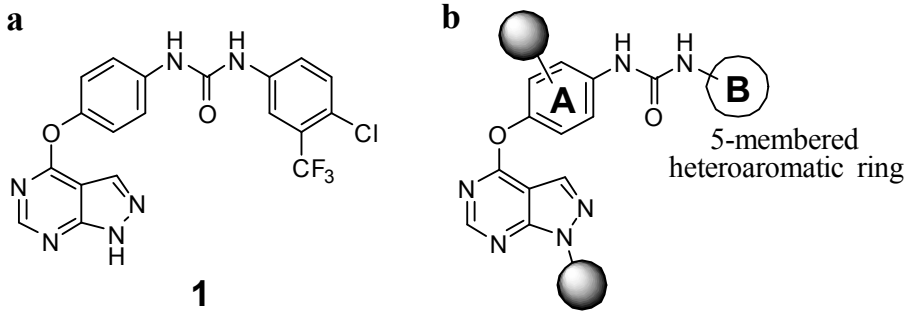

Figure 1. (a) Structure of compound **1**. (b) Schematic showing subgroups or atoms that were the focus of structural modifications.

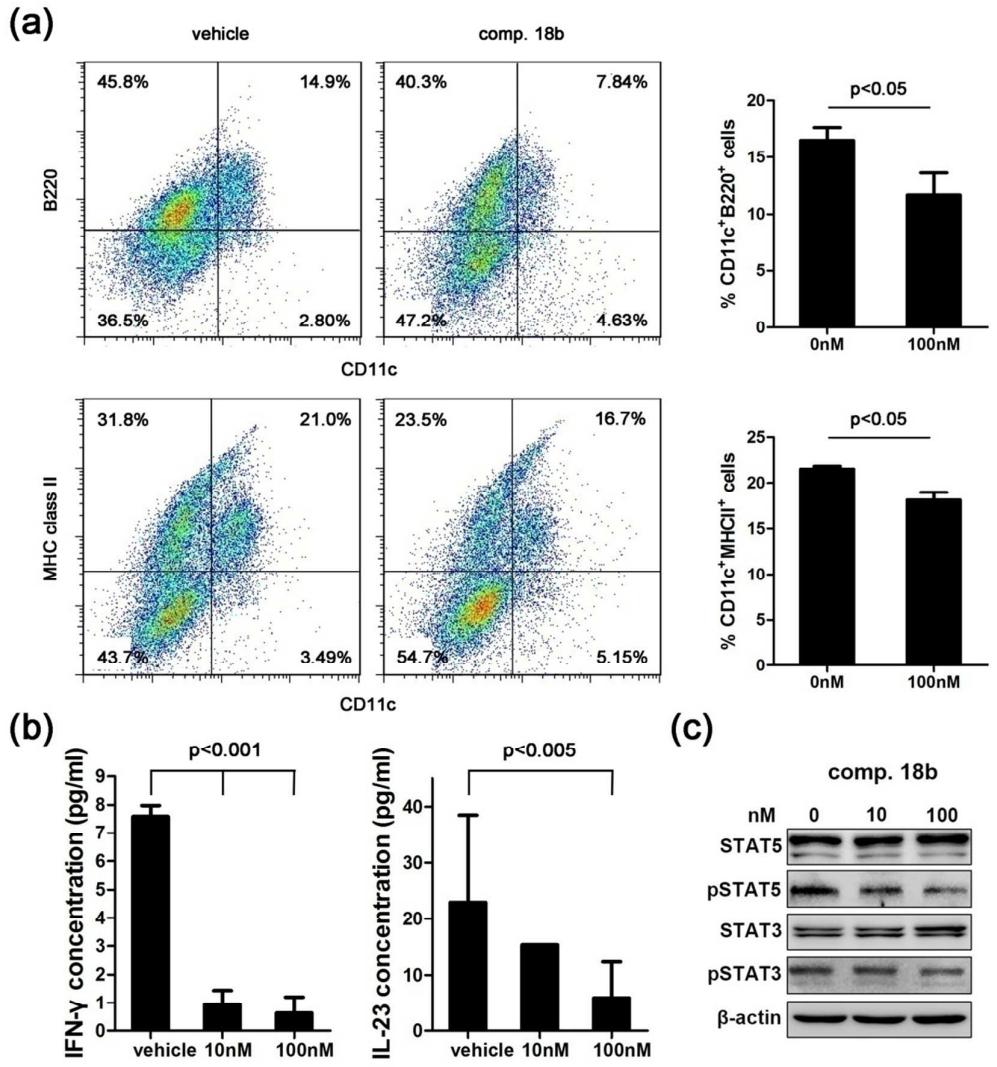

Figure 2. Compound **18b** showed considerable abilities to suppress the generation of DCs from BMDCs and inhibit cytokine secretion of DCs through the blockade of FLT3 signaling pathway *in vitro*. BM cells flushed from the femurs and tibias of BALB/c mice were cultured in RPMI 1640 medium supplemented with 10% FCS, 10^{-4} M 2-ME, sodium pyruvate, antibiotics, 100 nM FLT3L for 9 days. On 9th day, compound **18b** or 0.1% DMSO was added to the culture medium for 24 h (a), 12 h (b) and 1 h (c), followed by flow cytometric, Elisa and western blot assays as indicated. (a) Flow cytometric analysis of the $CD11c^+B220^+$ cells (pDCs) or the $CD11c^+$ MHC II^+ cells (mDCs). Representative flow cytometric analyses are shown; (b) IFN-γ and IL-23 in the supernatant were analyzed and quantified by Elisa; (c) Whole BM cells were lysed to evaluate the phosphorylation state of STAT3 and STAT5 by western blot. All the histogram shows the statistics data of three independent experiments.

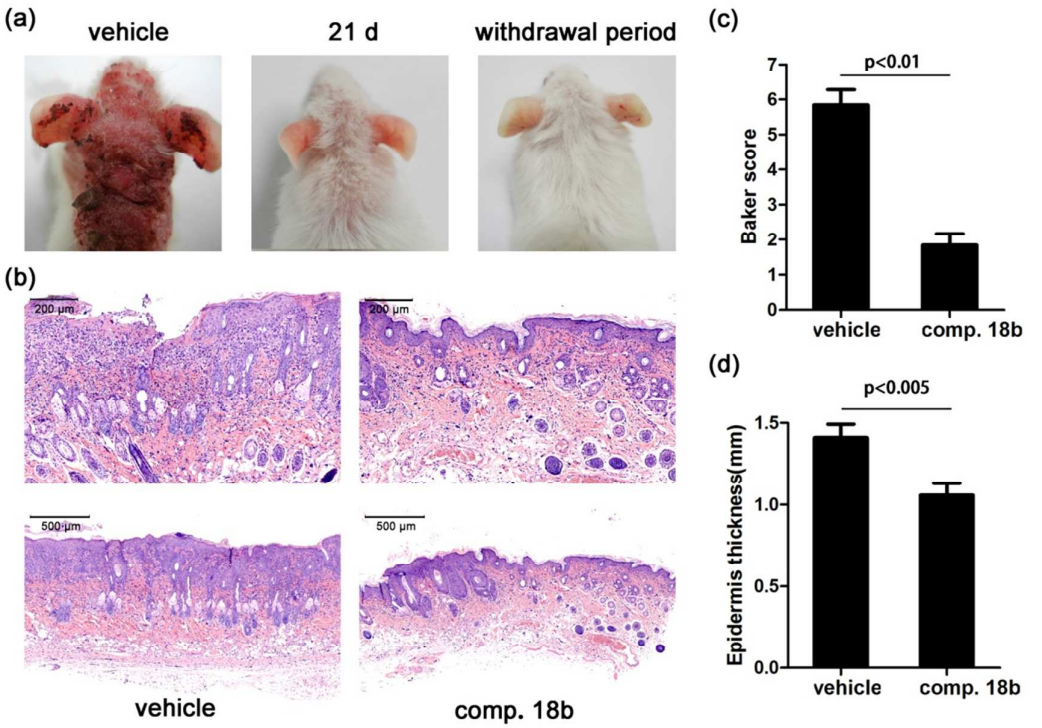

Figure 3. Anti-psoriatic activity of compound **18b** on K14-VEGF transgenic mice. K14-VEGF transgenic mice were treated as indicated in materials and methods section. (a) Macroscopic images of the mice after treatment with vehicle (left), compound **18b** (middle) and the mice 15 days after the last administration of compound **18b** (right); (b) HE staining of head and neck tissue sections after the treatment of compound **18b** for 29 days; (c) Quantitative assessments of the pathological score, based on the Baker score system, were performed in 5 randomly chosen fields. Mean scores and SD values are shown; (d) Epidermal thickness were measured in 8 randomly chosen fields (mean ± SEM).

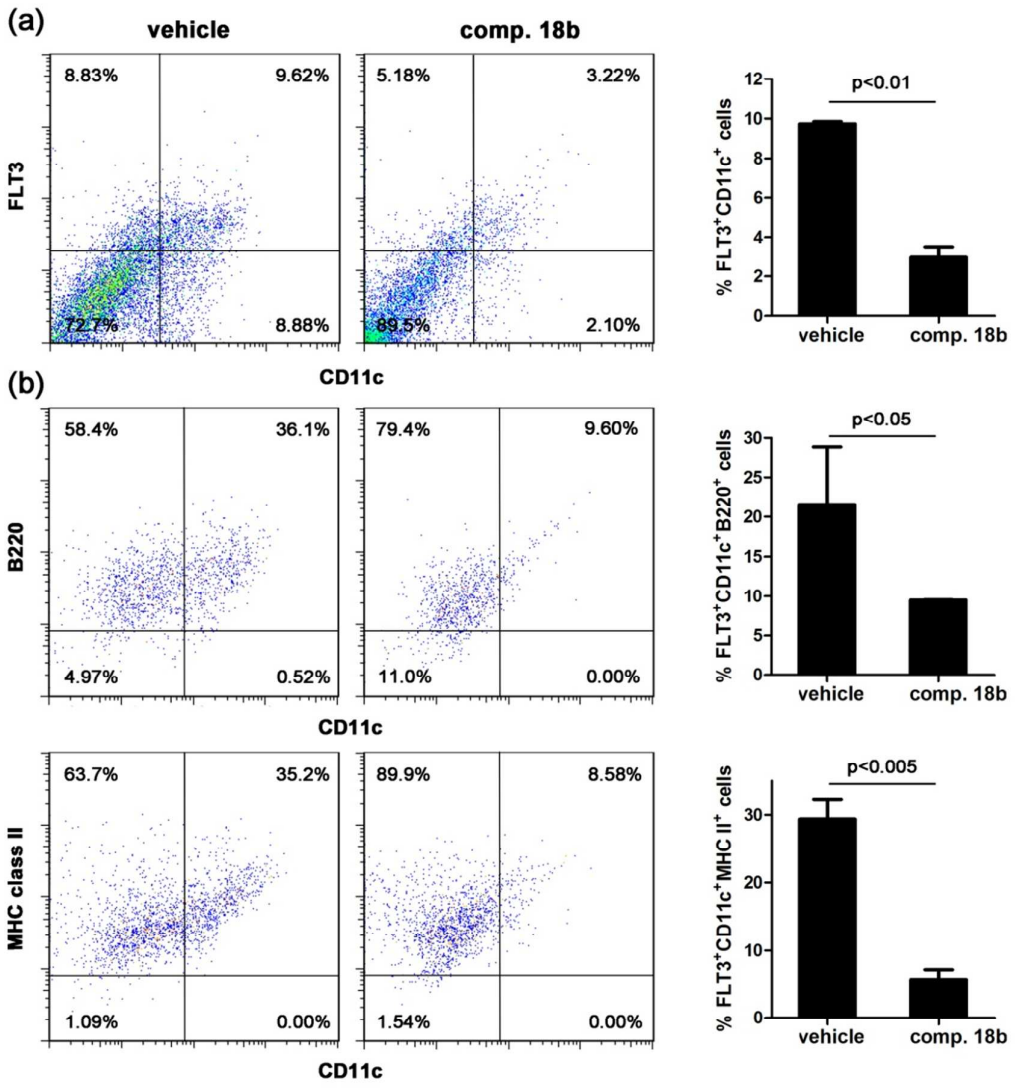

Figure 4. Flow cytometric quantification of $FLT3^+$ $CD11c^+$ DCs in single-cell suspensions isolated from vehicle-treated and compound **18b**-treatedpsoriatic plaque lesions. (a) Representative flow cytometric analyses of $FLT3^+$ $CD11c^+$ DCs are shown. (b) $FLT3^+$ cells were first gated and then plotted as CD11c versus B220 or MHC class II. Ordinates in the histogram indicate the percentage of each cell type within total skin cells. Data are representative of three independent experiments.

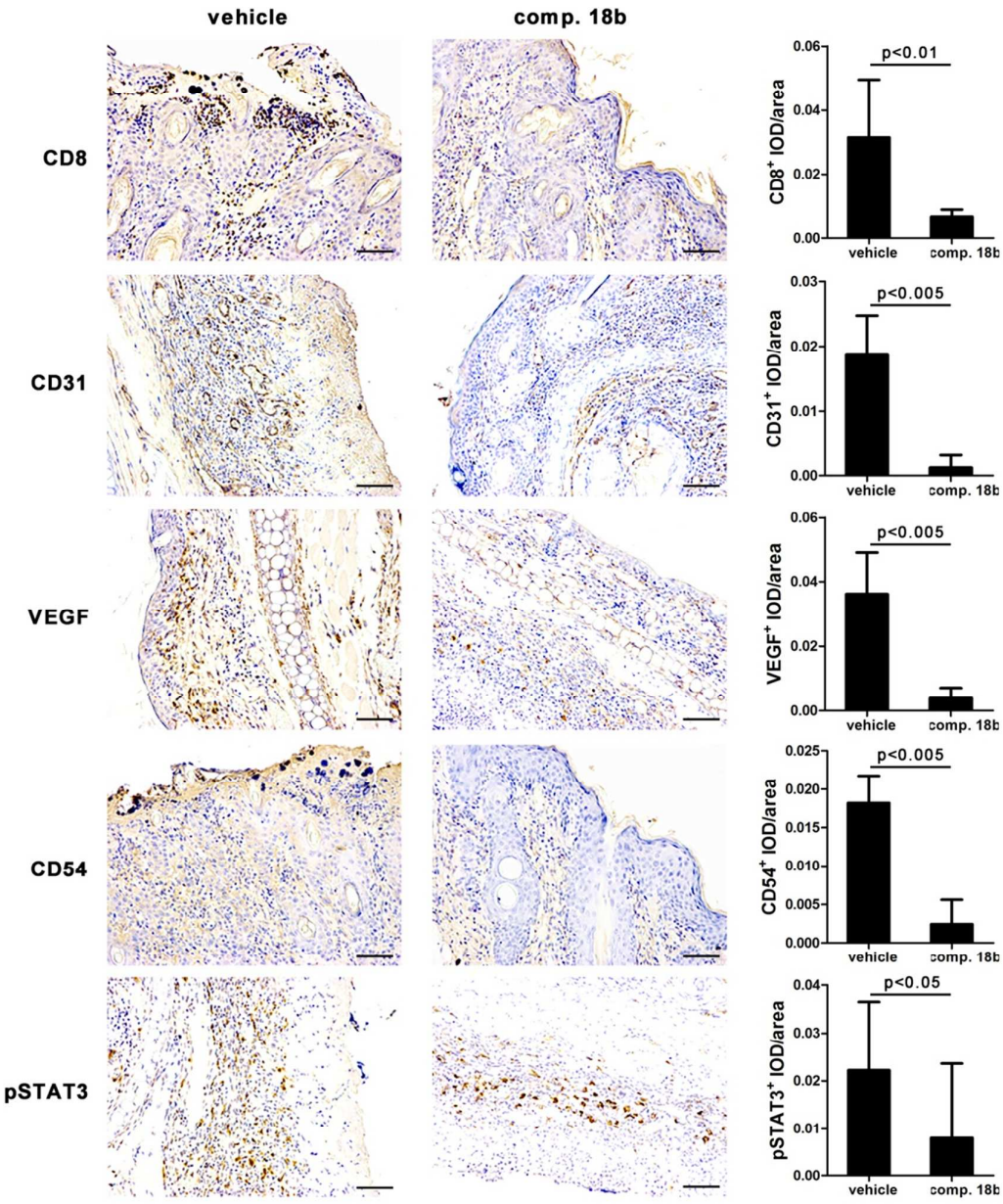

Figure 5. Immunohistochemical staining of tissue sections after treatments in a pharmacodynamic experiment. K14-VEGF transgenic mice were treated as indicated in Materials and Methods. After treatment 29 days, mice were killed, and 4-μm-thick paraffin-embedded ear skin sections were stained by immunohistochemistry to detect T lymphocyte infiltrationand related chemokines and growth factors in vehicle-treated and compound **18b**-treated mice. Quantitative immunohistochemical analysis were processed using the Imagepro Plus software in 5 randomly chosen fields and the data are shown in the histogram(mean ± SD, n=5 per group).

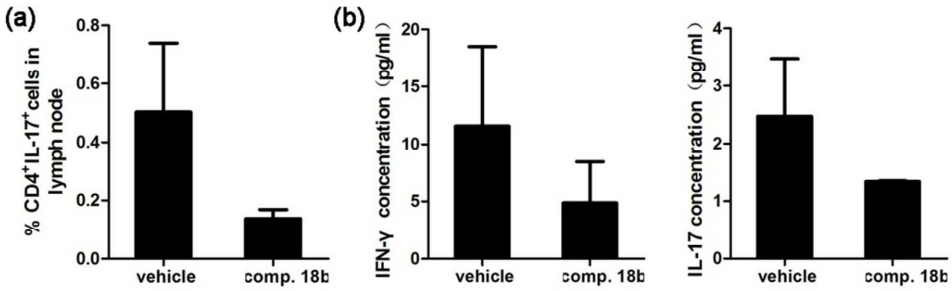

Figure 6. Inhibition of Th17/Th1 cells by compound **18b** treatment *in vivo*. Psoriasis model mice were treated with compound **18b** or vehicle for 29 days. (a) The lymph nodes were analysed by flow cytometry for Th17 cells ($CD4^+$ $IL\text{-}17^+$ cells). Data (mean ± SD) are representative of independent experiments using three mice; (b) The blood plasma was used for Elisa analysis of IL-17 and IFN-γ. Data (mean ± SD) are representative of independent experiments using three mice.

Table of Contents graphic